Amphiphilic Molecules Exhibiting Zwitterionic Excited-State Intramolecular Proton Transfer and Near-Infrared Emission for the Detection of Amyloid β Aggregates in Alzheimer's Disease

Zhengxin Yu,[a] Yusuff Moshood,[a] Marcin K. Wozniak,[b] Shrey Patel,[a] Karna Terpstra,[a] Daniel A. Llano,[c] Wawrzyniec Dobrucki,[b] and Liviu M. Mirica[a,d,*]

[a] Department of Chemistry, Beckman Institute for Advanced Science and Technology, The Neuroscience Program, University of Illinois at Urbana-Champaign, 600 S. Mathews Avenue, Urbana, Illinois 61801, United States

[b] Beckman Institute for Advanced Science and Technology, Department of Bioengineering, University of Illinois at Urbana-Champaign, Urbana IL 61801, United States

[c] Beckman Institute for Advanced Science and Technology, Department of Molecular and Integrative Physiology, University of Illinois at Urbana-Champaign, Urbana IL 61801, United States

[d] Hope Center for Neurological Disorders, Washington University School of Medicine, St. Louis, MO 63110, United States

* e-mail: mirica@illinois.edu

Abstract

Chromophores with zwitterionic excited-state intramolecular proton transfer (ESIPT) have been shown to have larger Stock shifts and red-shifted emission wavelengths compared to the conventional π-delocalized ESIPT molecules. However, there is still a dearth of design strategies to expand the current library of zwitterionic ESIPT compounds. Herein, we report a novel zwitterionic excited-state intramolecular proton transfer system enabled by addition of triazamacrocycle (TACN) fragments on a dicyanomethylene-4H-pyran (DCM) scaffold. The solvent-dependent steady-state photophysical studies and pKa measurements strongly support that the ESIPT process is more efficient with two TACN groups attached to the DCM scaffold and

not affected by polar protic solvents. Impressively, compound DCM-OH-2-DT emits with a near-infrared (NIR) emission wavelength at 740 nm along with an uncommonly large Stokes shift of ~ 280 nm. Moreover, DCM-OH-2-DT shows high affinity towards soluble amyloid β (Aβ) oligomers *in vitro* and in 5xFAD mouse brain sections, and we have successfully applied DCM-OH-2-DT for the NIR fluorescence *in vivo* imaging of Aβ aggregates and demonstrated its potential use as an early diagnostic agent for AD. Overall, this study can provide a general molecular design strategy for developing new zwitterionic ESIPT compounds with NIR emission for further *in vivo* imaging applications.

Keywords

Zwitterionic excited-state intramolecular proton transfer (ESIPT); Alzheimer's Disease; amyloid-β (Aβ) oligomers; early diagnosis; near-infrared (NIR) fluorescence imaging

Introduction

A unique four-level photochemical process that generates an intramolecular tautomer from the initial excited state upon proton transfer is called an excited-state intramolecular proton transfer (ESIPT). Ever since then the first report of ESIPT by Well et al. in the 1950s,[1] this photochemical process has been applied to a wide range of applications and has shown significant impact in various areas, including physiology, pharmacology, environmental science, chemical and bioimaging probes, as well as organic electronics and organic lasers.[2, 3] Conventionally, the majority of ESIPT molecules, such as derivatives of 2-(2'-hydroxyphenyl)benzothiazole (HBT), 2-(2'-hydroxyphenyl)benzimidazole (HBI), utilize π-delocalization for proton transfer at their excited states and exhibit an enol-to-keto phototautomerization process (Scheme 1A).[4, 5] Emerging evidence showed that besides the generation of the keto tautomer, a charge redistribution from the ESIPT process could lead to a zwitterionic form in the excited state.[6-9] For example, the zwitterionic excited states have been shown to exist for the following scaffolds: pyrrole-containing oligoarenes that involve a strap strategy with N−H···N-based hydrogen bonding (Scheme 1B);[6] a 3-thiolflavone platform with an excited-state intramolecular thiol S−H···O proton transfer (Scheme 1C);[7] and a traditional HBT platform but with two fluorene groups attached (Scheme 1D).[8] Interestingly, extremely large Stokes shifts and significant red-shifted emission wavelengths were observed from the zwitterionic ESIPT molecules, even when compared to the conventional π-delocalized ESIPT molecules.[7, 8] These large Stokes shifts and redshifts of the emission wavelengths are especially attractive features for chemical and biosensing and imaging applications. However, the dearth of strategies to develop such unique zwitterionic ESIPT molecules limit further exploration of their potential applications.

Protein misfolding and aggregation are highly associated with the progression of Alzheimer's Disease (AD), which is the most prevalent neurodegenerative disease.[10, 11] One hallmark of AD, the amyloid plaques, are formed from the aggregation of the beta-amyloid (Aβ) peptide.[12, 13] During the aggregation process, a variety of intermediate Aβ species exist, such as smaller soluble oligomers. These oligomers are found to be relevant in both the physiology and the pathology of AD.[14-16] Importantly, soluble Aβ oligomers dominate at the early stage of the

disorder; therefore, they could serve as a biomarker for early diagnosis of AD. However, due to the lack of an atomic structure for these oligomeric species, there is still great challenge to develop imaging agents targeting the soluble Aβ oligomers.[17, 18] Great efforts had been made in the past few decades to distinguish the different aggregation stages of the amyloid proteins.[19] For example, several oligomer-specific fluorescent probes,[20-25] probes based on restriction of the molecular rotation,[26, 27] and probes exhibiting FRET[28] were developed for Aβ oligomer detection. However, some of these probes have limited *in vivo* applications. Moreover, a ruthenium polypyridyl complex has also been designed and developed by Marti et al. for Aβ oligomer detection via photoluminescence anisotropy.[29] Recently, our group demonstrated that incorporating amphiphilic properties into small molecule design might increase their selectivity towards Aβ oligomers and hence will be beneficial for Aβ oligomer detection.[30, 31] Even though different strategies have been applied, *in vivo* imaging agents targeting Aβ oligomers are still highly needed, in order to expand the current toolbox of early diagnostic agents for AD.[32, 33]

Herein, we report a novel zwitterionic excited-state intramolecular proton transfer system enabled by triazamacrocycle (TACN) on a dicyanomethylene-4H-pyran (DCM) scaffold. From the solvent-dependent steady-state photophysical studies, density functional theory (DFT) calculations, and time-dependent DFT (TD-DFT) studies, we demonstrate that the zwitterionic ESIPT of DCM-OH-2-DT is more efficient than that of DCM-OH-2-MT, and this process is not affected by polar protic solvents. Moreover, the imaging applications of the developed compounds are further explored in an transgenic AD mouse model. With the hydrophilic TACN group(s) attached, the developed amphiphilic compounds were shown to be able to interact with the Aβ oligomers. *In vitro* binding affinity measurements and fluorescence brain section imaging studies indicate that the compounds have high affinity towards Aβ oligomers *in vitro* and can bind to the native Aβ aggregates on the transgenic AD mouse brain sections. Excitingly, we also demonstrate that compound DCM-OH-2-DT can readily penetrate the blood-brain barrier (BBB) and bind to native Aβ species. In real-time *in vivo* imaging studies, DCM-OH-2-DT showed significantly higher near-infrared (NIR) fluorescence intensity in the 5xFAD mice vs. wild-type (WT) controls. Lastly, we also show that the amphiphilic compounds can bind Cu(II) ions,

indicating their potential future use in ^{64}Cu positron emission tomography (PET) imaging of Aβ species in AD.

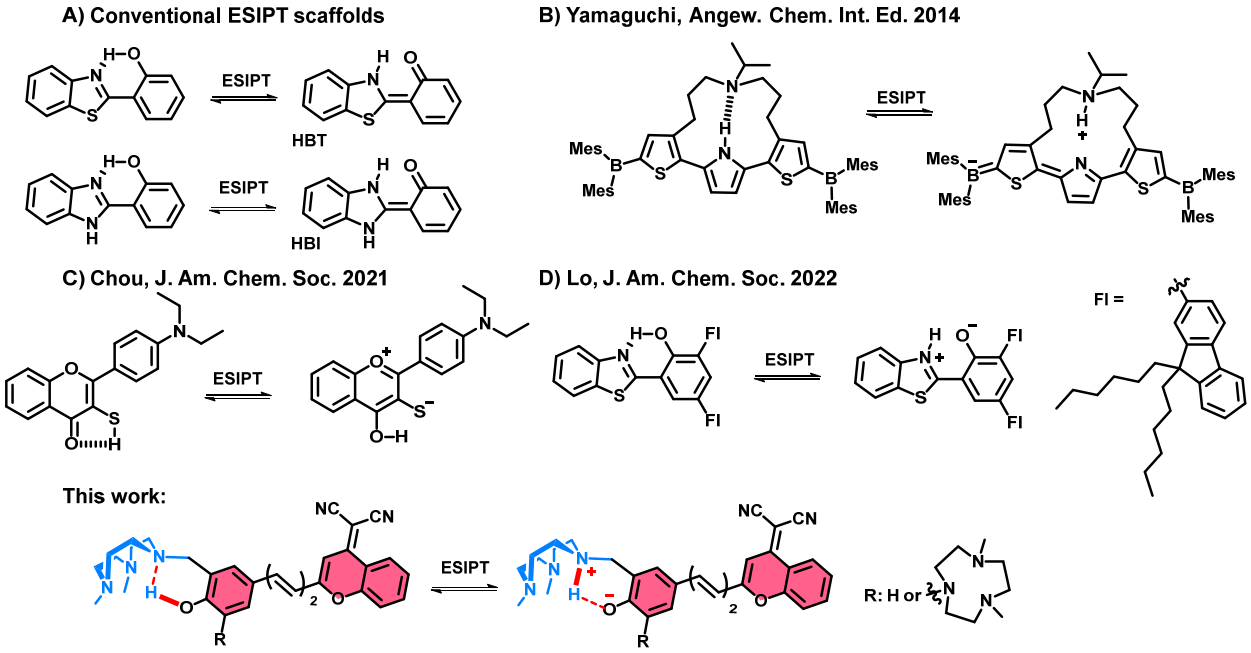

Scheme 1. Examples of ESIPT molecules.

Results and discussion

Zwitterionic Excited-State Intramolecular Proton Transfer Enabled by Azamacrocycles

It was reported by Yamaguchi and coworkers that an alkyl amino embed in an alkyl strap on the pyrrole-containing oligoarenes scaffold could facility the ESIPT process to generate zwitterionic ESIPT molecules.[6, 34] The hydrogen bonding interactions between the amino group and the pyrrole N-H proton, as well as the boryl groups serving as electron acceptors in the π-conjugated system, are the two critical components for their design. Even though it was reported that the ESIPT process was efficient in polar protic solvent, the applications in chemical/bio imaging of these developed zwitterionic ESIPT molecules are not explored, partially due to the difficulties for further chemical modifications. Therefore, we are motivated to explore the imaging applications for the unique zwitterionic ESIPT photochemical process via rational molecular engineering. Inspired by the previous strategy, we postulate that a labile hydrogen bond donor (e.g., phenol O-H proton), a D–π–A structure as the conjugated system to stabilize

the charge separated excited state, and an appropriate hydrogen bond acceptor are necessary to generate zwitterionic ESIPT molecules (Scheme 2a). Therefore, our molecular design focus on the following components: 1) a typical D–π–A structure is constructed by utilizing dicyanomethylene as the electron acceptor and phenol as the electron donor, which are linked via two C=C double bonds, 2) 2,4-dimethyl-1,4,7-triazacyclononane (Me_2HTACN) is chosen as a hydrogen bond acceptor and is installed ortho to the phenol group. Moreover, zero, one or two Me_2TACN groups are installed to compare and validate the ESIPT process. With this molecular design, three compounds were designed and synthesized: DCM-OH-2, DCM-OH-2-MT, and DCM-OH-2-DT (Scheme 2b). The synthetic details and spectroscopy characterizations (^{1}H, ^{13}C NMR, HPLC and HR-ESI) can be found in the Supporting Information.[35]

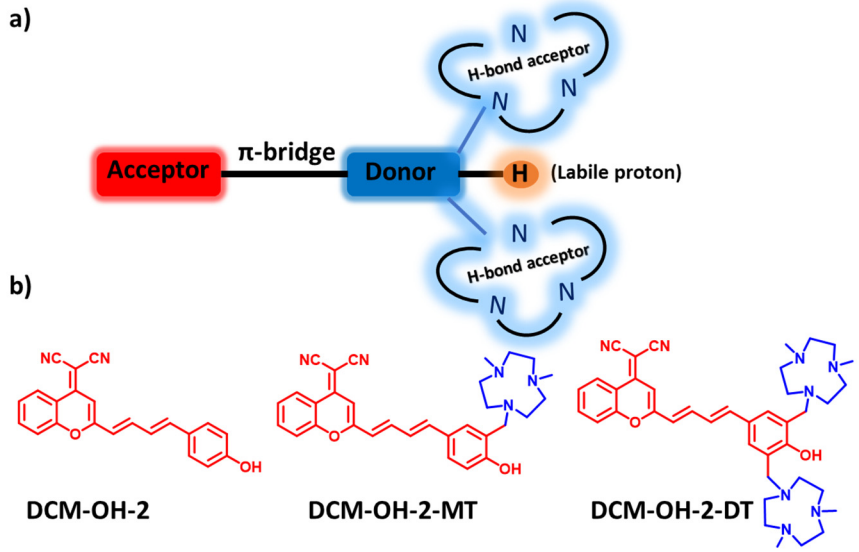

Scheme 2. a) Molecular design of the zwitterionic ESIPT molecule enabled by azamacrocycles. b) Chemical structure of DCM-OH-2, DCM-OH-2-MT and DCM-OH-2-DT.

When measuring the absorbance of the compounds in EtOH, there is no significant difference between the three compounds. They showed the maximum absorption at about 470 nm (Figure S1a). On the other hand, the emission bands were totally different for these compounds. Notably, for DCM-OH-2, the maximum emission locates at 625 nm. For DCM-OH-2-MT, two emission peaks at 615 nm and 740 nm were observed; and interestingly, only one emission peak locates at 740 nm for DCM-OH-2-DT (Figure 1a). Normally, two emission peaks from a locally excited (LE) state and an ESIPT state, are observed for the compounds that can go

through the ESIPT process.[36] Since two emission peaks were observed for DCM-OH-2-MT, one is similar to the DCM-OH-2 and another is the same as the DCM-OH-2-DT's peak, we believe with the TACN groups attached, DCM compounds would go through the ESPIT process to generate new zwitterionic species at the excited state like we originally proposed (Scheme 1). To further elucidate the differences on emission behaviors of these compounds, several experiments were performed. Firstly, the fluorescence excitation spectra for DCM-OH-2-MT were similar to its absorption spectra regardless of the 615 nm or 740 nm emission peak (Figure S1b). This indicates that the two emission peaks originate from the identical ground state. Secondly, the emission spectra of the compounds in several solvents with different polarities were recorded (Figure 1b). For DCM-OH-2, the maximum emission increases as the polarity of the solvent increases. Since DCM-OH-2 is built on the D–π–A scaffold, this solvation effects indicate the compounds would go through the intramolecular charge transfer (ICT) process at the excited state, which is a common feature for chromophores with donor-acceptor structures.[37] While for DCM-OH-2-MT, the two emission peaks vary dramatically in different solvents. In general, the compound emits with the longer emission in the solvent with lower polarity, such as toluene and THF. In polar protic solvent, such as MeOH and EtOH, the shorter emission appears as a shoulder peak, which is probably due to the intermolecular hydrogen bonding interactions with the protic solvent. Interestingly, for DCM-OH-2-DT, the emission wavelength is unaffected either by the polarity of the solvent or by the protic/aprotic properties of the solvent. This demonstrates that the ESIPT is more efficient for DCM-OH-2-DT compared to DCM-OH-2-MT.

The macrocycle TACN groups are close in proximity to the phenol group and can serve as proton sponge/hydrogen bond acceptors. As the formation of an intramolecular hydrogen bond is a prerequisite and can greatly affect the ESIPT process, we therefore investigated the effects of TACN groups on the hydrogen bond formation. From spectrophotometric titrations, we measured the acidity constant (pKa values) for the developed DCM compounds (Table S1 and Figure S2 and S3). Multiple pKa values were obtained for each compound, and the largest value was assigned to the phenol O-H due to the significant spectral changes (Figure 1c and 1d). With one TACN group attached, the pKa value decreased from 11.73 to 10.19 for DCM-OH-2-MT. Moreover, the pKa value was further decreased to 9.35 for DCM-OH-2-DT. This data indicates

that the acidity of the phenol proton increases in the presence of the TACN groups, which indirectly suggests the hydrogen bonding interactions between the phenol and TCAN groups. This intramolecular hydrogen bonding interactions in DCM-OH-2-DT are stronger than in DCM-OH-2-MT. It is also worth noting that the hydrogen bonding interactions between phenol and alkyl amino group at the ortho position was observed in the solid state for some metal chelators, such as carbohydrate-containing compounds.[38] Collectively, the data suggest that with two macrocycles attached, the ESIPT is more efficient and not affected by the polarity of solvent. This property is necessary and beneficial for their potential applications in physiological relevant aqueous conditions.

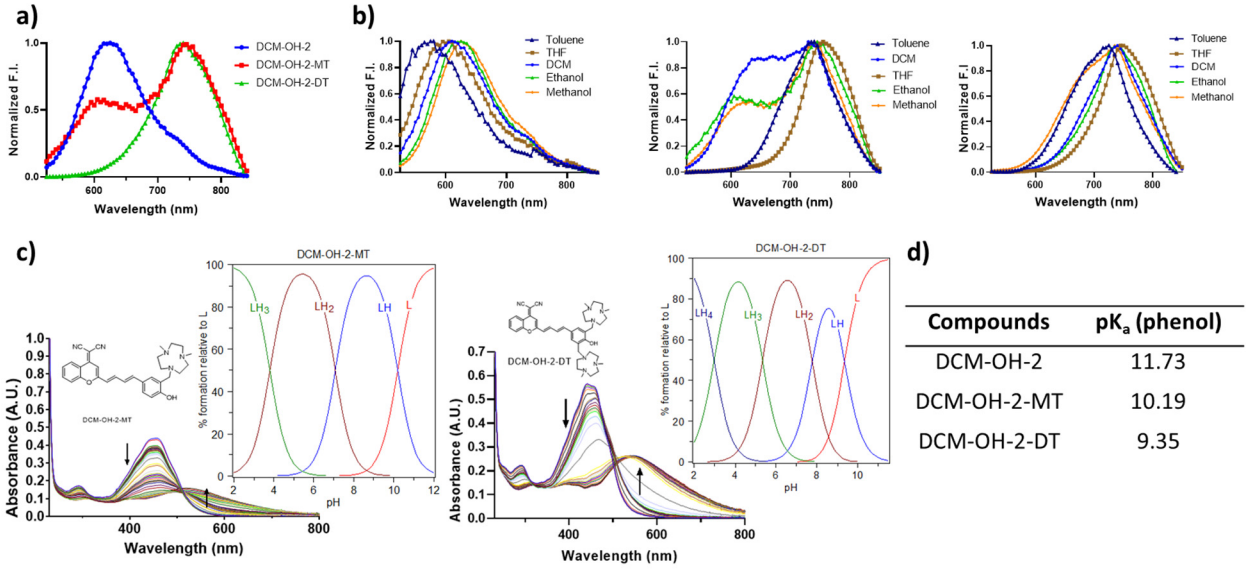

Compounds	pK_a (phenol)
DCM-OH-2	11.73
DCM-OH-2-MT	10.19
DCM-OH-2-DT	9.35

Figure 1. a) Emission spectra of the compounds (10 µM) in EtOH. b) Emission spectra of the compounds (10 µM) in different solvents: DCM-OH-2 (left), DCM-OH-2-MT (middle), and DCM-OH-2-DT (right). c) Variable pH (pH 3−11.0) UV−vis spectra of DCM-OH-2s compounds ([DCM-OH-2-MT] = 20 µM, [DCM-OH-2-DT] = 30 µM 25 °C, I = 0.1 M NaCl) and the corresponding species distribution plots. d) Calculated pKa values of the phenol groups for DCM-OH-2, DCM-OH-2-MT, and DCM-OH-2-DT obtained from the spectrophotometric titrations.

A series of density functional theory (DFT), and time-dependent DFT (TD-DFT) studies were performed to understand the electronic properties of the developed compounds. The optimized geometries for the frontier molecular orbitals were obtained using the B3LYP hybrid density functional along with the 6-31G+(d) basis set (Figure 2). The frontier molecular orbital analysis for the $S_0 \rightarrow S_1$ vertical excitations suggest that this transition corresponds to the HOMO

$\rightarrow$ LUMO transition. The HOMO and LUMO in DCM-OH-2 comprises the π and π^* molecular orbitals, whereas that of DCM-OH-2-MT and DCM-OH-2-DT are inherently the σ (non-bonding orbital) of TACN substituent and π^* orbital of the parent DCM-OH-2. The HOMO $\rightarrow$ LUMO transition energies in DCM-OH-2, DCM-OH-2-MT, and DCM-OH-2-DT are calculated to be +2.76 eV, +2.65 eV, and +2.51 eV, respectively (Figure S4). The progressive decrease in excitation energies is consistent with the observed experimental results. More detailed computational studies to probe the ESIPT process, from the S_1 state to the protonated forms of DCM-OH-2, DCM-OH-2-MT, and DCM-OH-2-DT are underway.

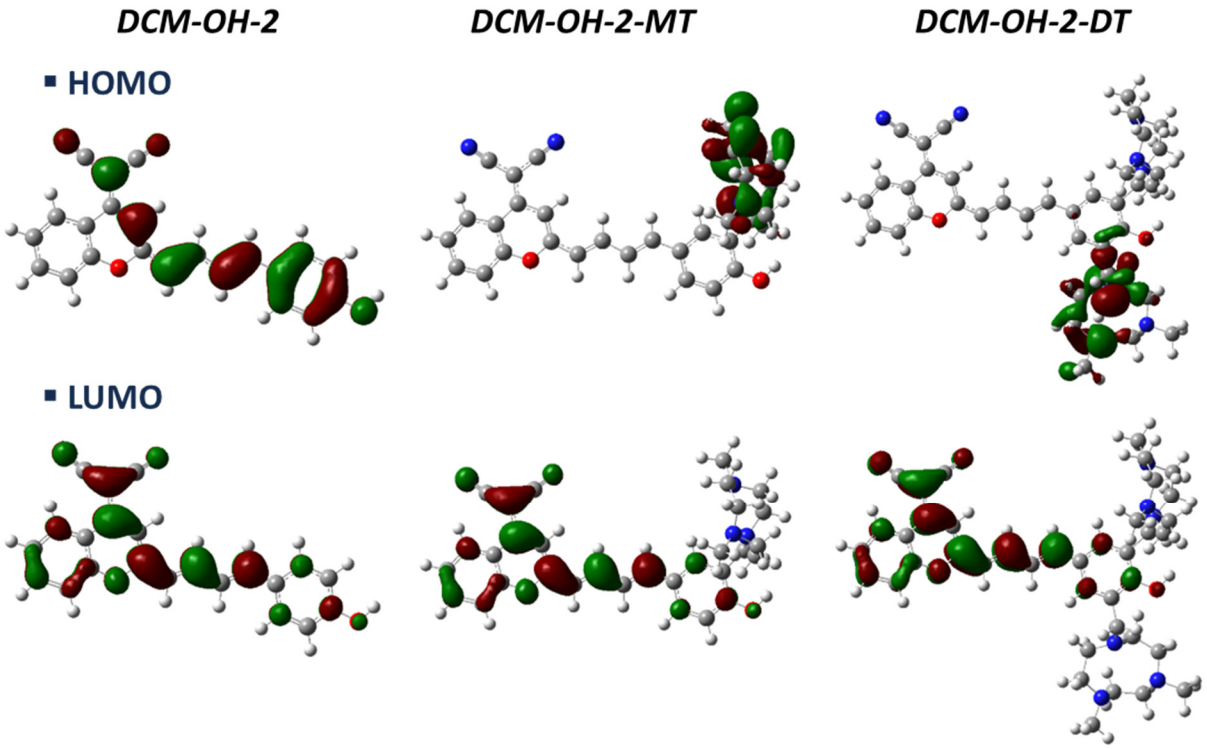

Figure 2. Depiction of the DFT-calculated (B3LYP/6-311G+) HOMOs and LUMOs of the three DCM-OH-2 compounds, shown as 0.05 isocontour plots.

In vitro Interactions Between the Amphiphilic DCM-RBFs and Amyloid β Aggregates

Inspired by the unique photophysical properties of these compounds, we aim to apply them for bioimaging studies. Our molecular design resembles some extended rotor-based fluorophores (RBFs), in which the electron donor and electron acceptor are linked via conjugated C=C double instead of C-C single bond. It was demonstrated that extended RBFs are capable of

detecting amyloid-oligomeric species formed during protein aggregation.[39] Moreover, some DCM derivatives were applied for Aβ aggregates detection in AD mouse model, while most of them are only reported for Aβ fibrils detection.[24, 40-42] Furthermore, with the hydrophilic TACN groups attached, the developed amphiphilic DCM compounds might have enhanced affinity/selectivity towards less aggregated oligomers.[30, 31] Therefore, we are encouraged to investigate the emission and binding properties of the newly developed DCM compounds on Aβ targeting, and their usage as *in vivo* early diagnostic agents.

To investigate the interactions between the compounds and Aβ aggregates, two types of Aβ aggregates (insoluble Aβ fibrils and soluble Aβ oligomers) were first prepared via synthetic Aβ monomers.[43] When compound DCM-OH-2 was incubated with Aβ aggregates in phosphate buffered saline (PBS), there is a significant fluorescence turn-on effect along with a shift in maximum emission wavelength from 680 nm to 620 nm (Figure 3a), indicating the binding mechanism of RBFs and the increased hydrophobicity at the binding pocket for DCM-OH-2. This dramatic blue shift in the emission wavelength makes DCM-OH-2 less ideal for *in vivo* imaging application since the emission wavelength is out of the NIR window (>650 nm). Due to the increased hydrophobicity at the binding site, a hypochromic shift is commonly observed for a variety of Aβ targeting probes and makes their *in vivo* applications limited.[44] Interestingly, DCM-OH-2-DT not only exhibited fluorescence enhancement, but also showed unchanged maximum emission wavelength at about 730 nm in the presence of Aβ aggregates (Figure 3a). However, DCM-OH-2-MT exhibited two emission peaks, one peak located at 620 nm could be attributed to LE (which was observe with DCM-OH-2) and the other peak at 730 nm (similar to DCM-OH-2-DT) could be originated from the ESIPT emission (Figure 3a). These emission differences further confirmed that with two TACN groups attached, the ESIPT process is not affected by the polarity of the surrounding environment (binding pockets of the protein of interest (POI)). At the same time, we are also aware that the amphiphilic DCM compounds might bind to a different site compared to DCM-OH-2 given the extra hydrophilic interactions from the TACN groups. Nevertheless, the long emission wavelength and turn-on effects make DCM-OH-2-DT a good candidate for further *in vivo* imaging studies. Before moving forward, we also systematically investigated the effects of number of double bonds on Aβ targeting abilities. We synthesized and

characterized DCM-OH-1s and DCM-OH-3s, which has one and three double bonds, respectively (Scheme S2 and S3). Interestingly, DCM-OH-1-MT and DCM-OH-1-DT showed fluorescence enhancement in the presence of Aβ aggregates, while their maximum emission locate at the edge of NIR window (~650 nm, Figure S4). DCM-OH-3-MT and DCM-OH-3-DT didn't exhibit fluorescence turn-on effects in the NIR region (Figure S5).

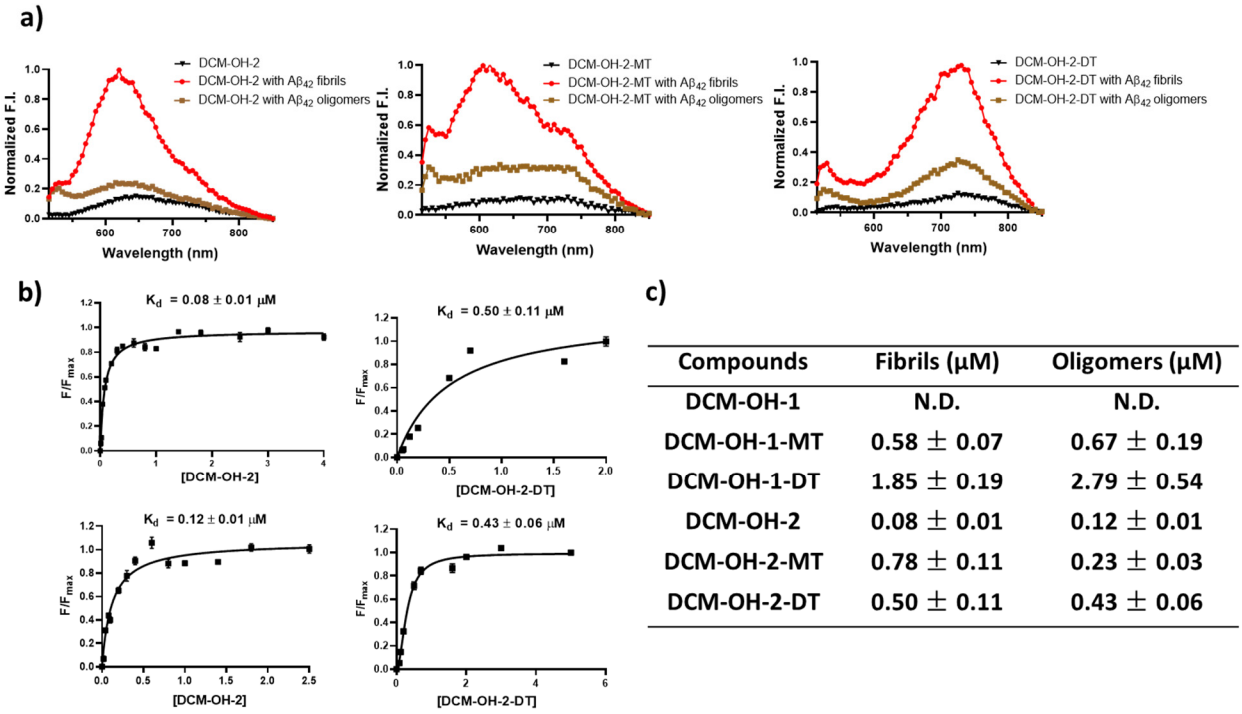

Compounds	Fibrils (μM)	Oligomers (μM)
DCM-OH-1	N.D.	N.D.
DCM-OH-1-MT	0.58 ± 0.07	0.67 ± 0.19
DCM-OH-1-DT	1.85 ± 0.19	2.79 ± 0.54
DCM-OH-2	0.08 ± 0.01	0.12 ± 0.01
DCM-OH-2-MT	0.78 ± 0.11	0.23 ± 0.03
DCM-OH-2-DT	0.50 ± 0.11	0.43 ± 0.06

Figure 3. a) Fluorescence turn-on effects with $A\beta_{42}$ oligomers and fibrils. Left: DCM-OH-2, middle: DCM-OH-2-MT, and right: DCM-OH-2-DT. Black: compound only; Brown: compound + $A\beta_{42}$ oligomers; Red: compound + $A\beta_{42}$ fibrils; [compound] = 5 μM; [$A\beta_{42}$ oligomers] = 25 μM; [$A\beta_{42}$ fibrils] = 25 μM. b) Binding constant measurements of DCM-OH-2 (left), DCM-OH-2-DT (right) with $A\beta_{42}$ fibrils (top), and oligomers (bottom). The K_d curves were fitted in GraphPad Prism with one site-specific binding model. Equation: Y = Bmax*X/ (Kd +X). c) Summarized K_d values for the DCM-based compounds (see other fitting curves in SI). N.D.: not determined. All measurements were conducted in PBS (10 mm, pH 7.4).

Furthermore, the binding affinities were obtained via fluorescence saturation assays for the developed compounds (Figure 3b, 3c, Figure S6 and S7). Excitingly, compounds with two double bonds (DCM-OH-2s) showed higher affinities comparing to compounds with one double bond (DCM-OH-1s), and DCM-OH-2 showed extremely higher affinities towards both Aβ fibrils (about 80 nM) and Aβ oligomers (about 120 nM). For DCM-OH-2-MT, the affinity towards Aβ

oligomers (about 230 nM) is about three time higher than its affinity towards Aβ fibrils (about 780 nM). This data supports and matches with our previously finding that incorporating amphiphilicity into small molecules might enhance their selectivity towards Aβ oligomers. We observed that DCM-OH-2-DT though still favor Aβ oligomers over Aβ fibrils, it showed a slightly lower affinity towards Aβ oligomers (about 430 nM) compared to DCM-OH-2-MT, and we postulate that this could be due to the increased steric hindrance. Form our structure-activity studies, we demonstrated that the idea binding pockets suit best for the DCM compounds with two doubles, and the length of conjugation was calculated to be about 12.07 Å for DCM-OH-2s, which might help to future design of the π-conjugated donor-acceptors molecules. Taken together, the low K_d value of DCM-OH-2-DT and extremely long emission support the binding and targeting abilities towards Aβ oligomers, which is essential for further *in vivo* studies.

Early Detection of Low-Viscosity Misfolded Oligomers In Vitro with Amphiphilic DCM-RBFs

Since the DCM-OH-2s have the desired emission and Aβ binding properties, the following studies mainly focus on the DCM-OH-2-based compounds. It was demonstrated that RBFs with high viscosity sensitivity only emit strong fluorescence in a high viscous environment such as insoluble aggregates, while RBFs with low viscosity sensitivity can maintain strong fluorescence in misfolded oligomers with low viscosity.[39] Therefore, we evaluated the viscosity sensitivity of the DCM-based RBFs and investigated their performances in monitoring Aβ aggregation *in vitro*. Firstly, the fluorescence intensities of these RBFs were obtained in a series of mixtures of ethylene glycol and glycerol. Based on the Föster-Hoffmann equation $\log(I) = x\log(\eta) + C$, the slope (x value) for each DCM RBFs was generated via a linear fitting.[45] The larger the x value is, the higher viscosity sensitivity the compound has. DCM-OH-2s compounds showed much lower x values comparing to Thioflavin T (ThT) (Figure 4a and 4b), a well-known RBF for well-aggregated amyloid fibrillar structures.[46, 47] Compound DCM-OH-2-DT exhibited the lowest viscosity sensitivity and is less sensitive to viscosity change compared to the asymmetric DCM-OH-2-MT, which is probably due to its higher energy barrier for the twisted-intramolecular charge transfer (TICT) process. DCM-OH-2 and DCM-OH-2-DT were then applied to monitor the aggregation of $A\beta_{42}$ peptide since they have lower x values. In this experiment, ThT showed minimal

fluorescence enhancement from 0–10 h, mainly because ThT cannot detect less aggregated oligomers that are formed rapidly from the monomeric peptide. In contrast, DCM-OH-2 and DCM-OH-2-DT showed more significant fluorescence increasement at the early stage of the aggregation process (Figure 4c). Further fluorescence enhancement was observed till 40 h indicating the formation of well aggregated Aβ fibrils. Taken together, we believe the developed DCM-based RBFs with low viscosity sensitivity have the potential to be used as early diagnostic agents detecting oligomeric Aβ aggregates.

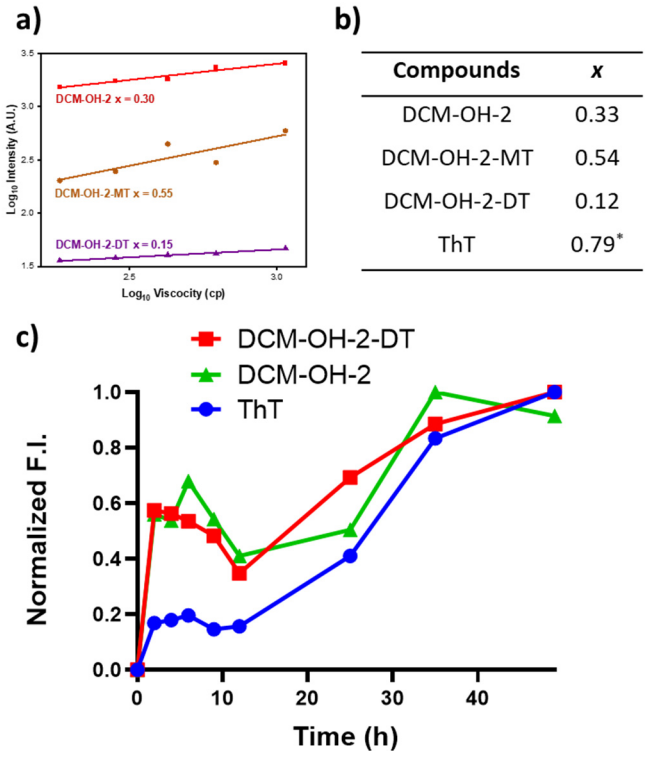

Figure 4. a) Viscosity sensitivity measurement of compound DCM-OH-2, DCM-OH-2-MT and DCM-OH-2-DT in ethylene glycol and glycerol mixture. Liner fitting based on equation: log(I) = xlog(η) +C. b) Summarized Viscosity sensitivity values obtained from the slope (x) of the liner fitting. c) Detection of $A\beta_{42}$ aggregation by ThT, DCM-OH-2 and DCM-OH-2-DT. * From Ref [39].

Detection of Native Aβ Aggregates with Amphiphilic DCM-RBFs

After demonstrating the *in vitro* interactions between the DCM-based RBFs with Aβ aggregates, we then investigated their interactions with native Aβ aggregates on 5xFAD mouse brain sections. 5xFAD mouse is commonly used as AD mouse model, that will generate and

accumulate various Aβ aggregates in the brain.[48] Individual brain slices with 40 μm thickness sectioned from 9-month-old AD brains were applied for the staining experiment. ThS, which is widely used to label *ex vivo* Aβ aggregates on mouse brain section, was applied in the colocalization experiments (Figure 5a).[49] Compound DCM-OH-2 colocalized with ThS extremely well in the core regions of the aggregates, which represent the more condensed and heavily aggregates fibrillar species.[50] Interestingly, for compounds DCM-OH-2-MT and DCM-OH-2-DT, they bind to the peripheral region of the aggregates and surround the signals from ThS. The peripheral regions of Aβ aggregates on the brain sections were shown to be less aggregated oligomeric Aβ species.[20] From these labeling results, compared to ThS and DCM-OH-2, amphiphilic compoundsDCM-OH-2-MT and DCM-OH-2-DT were shown to prefer and are also able to interact with native oligomeric Aβs. To serve as imaging agents for *in vivo* studies, these compounds should also be able to cross BBB readily. The lipophilicity of the compounds was measured via partition coefficient measurements and these compounds showed LogD value between 0.9 to 1.7 (Table S2), indicating their potentials to cross BBB.[51] Indeed, when 5xFAD mice were treated with DCM-OH-2-DT for 10 days, we observed the brain accumulation of the compound bound to Aβ aggregates, which is further confirmed by the post-colocalization experiments with ThS (Figure 5b). These results strongly suggest that the compound can successfully cross the BBB and bind to the native Aβ species.

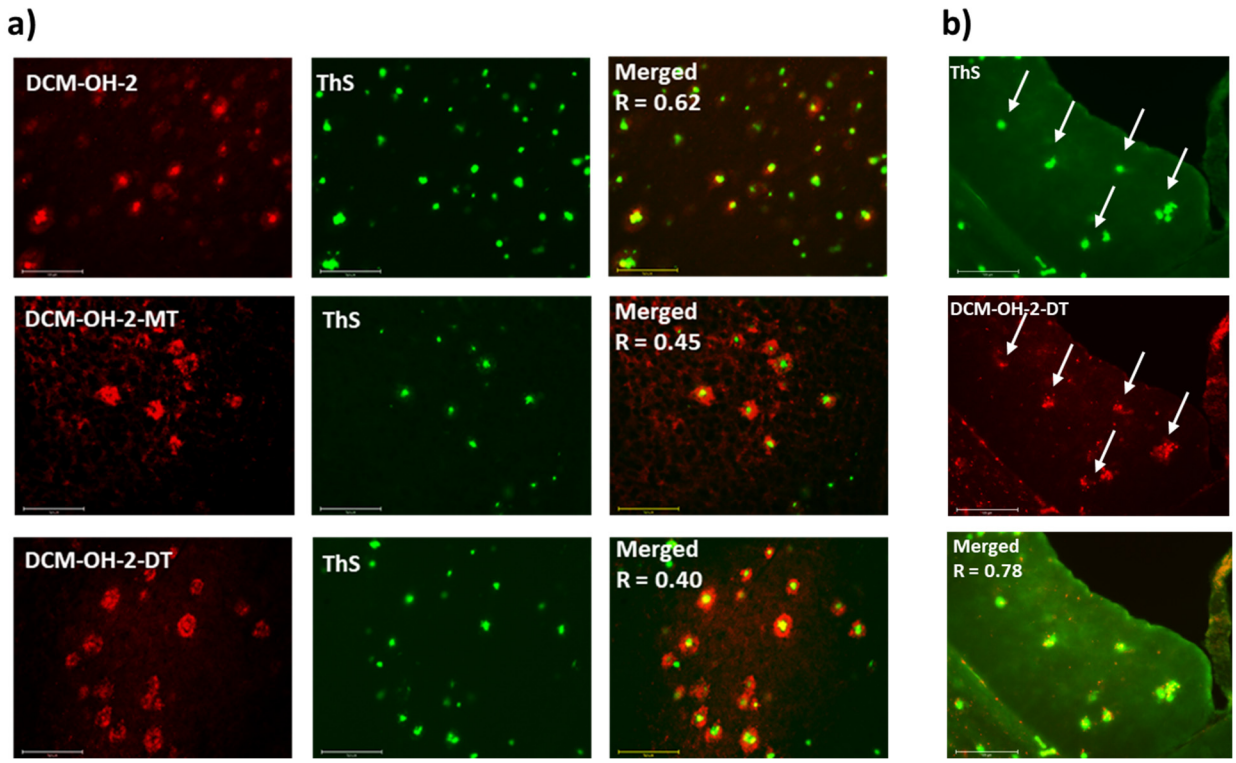

Figure 5. a) Fluorescence microscopy images of 9-month-old 5xFAD mice brain sections co-incubated with the DCM-based compounds (left), ThS (middle) and merged images (right, along with the Parson's correlation coefficients R). Concentrations: [compound] = 10 µM, [ThS] = 2.5 µM; scale bar: 125 µm. b) Brain sections were collected from 12-month-old AD treated with the DCM-OH-2-DT for 10 days at 1 mg/Kg. Fluorescence microscopy images of the brain sections stained with ThS. Conditions: [ThS] = 5 µM, scale bar: 125 µm.

Real-time *In vivo* Imaging with Amphiphilic DCM-RBFs

With the promising results, we are motivated to explore the *in vivo* imaging capabilities of the developed compounds. The cytotoxicity of the DCM compounds towards different neuro cells, mouse neuroblastoma (N2A) and human neuroblastoma (SH-SY5Y) cells, was first validated. In general, DCM derivates behaves similarly and induced no obvious cytotoxicity to both cells (Figure S8 and S9). DCM-OH-2 is slightly more toxic than the others, possibly due to its poor solubility in the cell media. This also emphasizes the importance of the hydrophilic TACN groups, which help to increase the hydrophilicity of the compounds; and therefore, improve their *cellular* and *in vivo* performance. Based on all the above studies, DCM-OH-2-DT was chosen as the best candidate for the real-time *in vivo* fluorescence imaging studies. 7-month-old AD mice and age-matched wild-type (WT) mice were injected with the compound at 5 mg/Kg. NIR fluorescence

intensity from the brain region were collected and analyzed over the course of time. The signal from DCM-OH-2-DT increase to the maximum about 15 min after the injection, followed by a slow clearance of the compound. When comparing the signal intensity with WT mice, excitingly, DCM-OH-2-DT exhibited significantly higher fluorescence signal in AD mice at 5-, 15-, 30-min post injection (Figure 6a and 6b). These imaging results further support the potentials *in vivo* application of the developed compounds. Additionally, DCM-OH-2-DT being able to differentiate the AD mice vs WT at a relative early age (7-month-old) also suggests the potential application as an early diagnostic agent for AD.

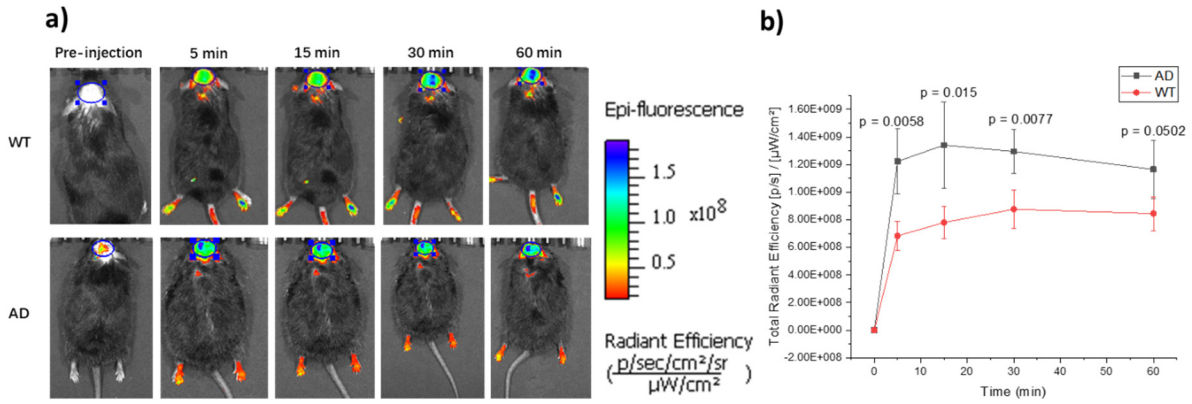

Figure 6. a) Representative images of 5xFAD mice and control mice at different time points before and after injection of the compound DCM-OH-2-DT (5mg/Kg). b) Quantitative analysis of fluorescence signals in the brain region from transgenic 5xFAD mice and control mice (n = 3) at preinjection and 5, 15, 30, 60 mins after injection. The signals were significantly higher in 7-mo-old 5xFAD mice than in the age-matched control mice. P values were calculated by Student's t test.

Cu Chelating Abilities of the Amphiphilic DCM-RBFs

Macrocyclic TACN serves as a common ligand framework to chelate Cu and is widely used in ^{64}Cu-based PET imaging for various diseases. Our group demonstrated that phenol with Me_2TACN or other TACN derivatives are able to chelate ^{64}Cu efficiently and strongly.[52-54] However, the Cu chelating abilities of phenol with two TACN groups attached have never been investigated. Job's plots were first performed to analyze the stoichiometry of the Cu(II)−ligand in solution. For DCM-OH-1-MT and DCM-OH-1-DT, the breaks in the plots occur in between 0.33 and 0.5 Cu mole fraction indicating a mixture of 1:1 and 2:1 ligand to Cu complexes in solution while for DCM-OH-2-DT, the major 1:1 ligand to Cu complexes were observed (Figure S10). We

postulate that the electron donating ability of the phenol groups affected by the numbers of double can lead to the stoichiometry difference of the Cu(II)−ligand in solution. Furthermore, spectrophotometric titrations were performed on the Cu(II) complexes to determine the corresponding stability constants (Figure S11 and S12). Interestingly, DCM compounds with one double bond showed higher affinities (Log K) towards Cu, about ∼ 1 or 2 orders of magnitude larger than that of DCM compounds with two double bonds (Table 1). Moreover, DCM-based compounds with two TACN groups attached also showed higher stabilities constant than the MT-based compounds, which is probably due to the extra chelating abilities of the TACN group (Table 1). Finally, the concentrations of free Cu(II) (pM = $-\log[M_{unchelated}]$) at a specific pH value can be calculated from the speciation plots. The calculated pCu values with 1:1 ligand to Cu ratio for the DCM compounds at pH 6.6 and pH 7.4 are also comparable to the strong Cu chelating agent DTPA (Table S3).[55] Overall, we demonstrated that the amphiphilic DCM compounds can chelate Cu strongly and have the potential to be used as ^{64}Cu chelating agents for PET imaging of AD.

Table 1. Summarized stability constants (Log K) for the ligand-Cu(II) complexes

	DCM-OH-1-MT	DCM-OH-1-DT	DCM-OH-2-MT	DCM-OH-2-DT
$\mathbf{M^{2+} + HL^{+} = [MHL]^{3+}}$	4.86(2)	6.39(7)	5.32(3)	5.29(5)
$\mathbf{M^{2+} + L = [ML]^{2+}}$	**14.13(1)**	**16.57(3)**	**13.14(2)**	**13.62(3)**
$\mathbf{[ML(H_2O)]^{2+} = [ML(OH)]^{+} + H^{+}}$			4.62(3)	6.72(3)

Conclusions

In summary, we have developed a new zwitterionic ESIPT system enabled by triazamacrocycle (TACN) groups attached to the DCM scaffold. Interestingly, with two TACN groups attached, the zwitterionic ESIPT process is extremely efficient, even in physiological relevant aqueous media. The imaging applications of the developed compounds were further investigated in the context of AD. We successfully demonstrated that compound DCM-OH-2-DT binds to Aβ oligomers *in vitro* and to the native Aβ aggregates *in vivo*. Utilizing the long emission (740 nm) from the zwitterionic excited-state, DCM-OH-2-DT exhibited significant higher fluorescence intensity in the AD mice vs. age-matched WT mice in real-time *in vivo* imaging

studies. We also showed that DCM-OH-2-DT is a strong chelator for Cu and has the potential to be labeled with ^{64}Cu, to serve as a potential ^{64}Cu PET imaging agent for AD. We believe the dual-imaging capabilities of the compound will benefit both preclinical and clinical studies for AD. Finally, our molecular design could be a generalizable strategy for developing zwitterionic ESIPT molecules with different photophysical properties and applications. Further tuning of the photophysical properties of this molecules includes the substitution of the electron acceptor (dicyanomethylene) or the electron donor (phenol group) with other strong electron withdrawing groups or hydrogen bond donors (such as aniline with the labile N-H proton).[56] In addition, to expand the functionality of these molecules, the phenol group could be readily capped with a variety of triggers that could be reactive only in presence of specific analytes, to generate various reactivity-based imaging agents.[57, 58] Further studies regarding the effect of the number of nitrogen atoms on the macrocycle and the substituents on the amino group are currently ongoing in our group.

Conflicts of interest

A provisional patent (U.S. Patent Application No. 63/389,270, Title: "Amphiphilic Compounds for attenuating neurotoxicity of amyloid-beta oligomers and diagnostic methods", Inventors: Liviu M. Mirica and Zhengxin Yu, Filing date: July 14, 2022) has been filed on the synthesis and applications of the compounds described herein. All authors declare no other competing interests.

Acknowledgments

This work was supported by research funding from the NIH (R01GM114588 to L.M.M.).

ORCID

Liviu Mirica: 0000-0003-0584-9508

Zhengxin Yu: 0000-0002-3592-9704

References

1. Weller, A., Über die Fluoreszenz der Salizylsäure und verwandter Verbindungen. *Naturwissenschaften* **1955,** *42* (7), 175-176.
2. Sedgwick, A. C.; Wu, L.; Han, H.-H.; Bull, S. D.; He, X.-P.; James, T. D.; Sessler, J. L.; Tang, B. Z.; Tian, H.; Yoon, J., Excited-state intramolecular proton-transfer (ESIPT) based fluorescence sensors and imaging agents. *Chem. Soc. Rev.* **2018,** *47* (23), 8842-8880.
3. Padalkar, V. S.; Seki, S., Excited-state intramolecular proton-transfer (ESIPT)-inspired solid state emitters. *Chem. Soc. Rev.* **2016,** *45* (1), 169-202.
4. Henary, M. M.; Wu, Y.; Fahrni, C. J., Zinc(II)-Selective Ratiometric Fluorescent Sensors Based on Inhibition of Excited-State Intramolecular Proton Transfer. *Chem. Eur. J.* **2004,** *10* (12), 3015-3025.
5. Barman, S.; Mukhopadhyay, S. K.; Gangopadhyay, M.; Biswas, S.; Dey, S.; Singh, N. D. P., Coumarin–benzothiazole–chlorambucil (Cou–Benz–Cbl) conjugate: an ESIPT based pH sensitive photoresponsive drug delivery system. *J. Mat. Chem. B* **2015,** *3* (17), 3490-3497.
6. Suzuki, N.; Fukazawa, A.; Nagura, K.; Saito, S.; Kitoh-Nishioka, H.; Yokogawa, D.; Irle, S.; Yamaguchi, S., A Strap Strategy for Construction of an Excited-State Intramolecular Proton Transfer (ESIPT) System with Dual Fluorescence. *Angew. Chem. Int. Ed.* **2014,** *53* (31), 8231-8235.
7. Wang, C.-H.; Liu, Z.-Y.; Huang, C.-H.; Chen, C.-T.; Meng, F.-Y.; Liao, Y.-C.; Liu, Y.-H.; Chang, C.-C.; Li, E. Y.; Chou, P.-T., Chapter Open for the Excited-State Intramolecular Thiol Proton Transfer in the Room-Temperature Solution. *J. Am. Chem. Soc.* **2021,** *143* (32), 12715-12724.
8. Shukla, A.; Mai, V. T. N.; Divya, V. V.; Suresh, C. H.; Paul, M.; Karunakaran, V.; McGregor, S. K. M.; Allison, I.; Narayanan Unni, K. N.; Ajayaghosh, A.; Namdas, E. B.; Lo, S.-C., Amplified Spontaneous Emission from Zwitterionic Excited-State Intramolecular Proton Transfer. *J. Am. Chem. Soc.* **2022,** *144* (30), 13499-13510.
9. Mutai, T.; Tomoda, H.; Ohkawa, T.; Yabe, Y.; Araki, K., Switching of Polymorph-Dependent ESIPT Luminescence of an Imidazo[1,2-a]pyridine Derivative. *Angew. Chem. Int. Ed.* **2008,** *47* (49), 9522-9524.

10. Hardy, J.; Selkoe, D. J., The Amyloid Hypothesis of Alzheimer's Disease: Progress and Problems on the Road to Therapeutics. *Science* **2002,** *297* (5580), 353-356.
11. Spillantini, M. G.; Schmidt, M. L.; Lee, V. M. Y.; Trojanowski, J. Q.; Jakes, R.; Goedert, M., α-Synuclein in Lewy bodies. *Nature* **1997,** *388* (6645), 839-840.
12. Karran, E.; Mercken, M.; Strooper, B. D., The Amyloid Cascade Hypothesis for Alzheimer's Disease: An Appraisal for the Development of Therapeutics. *Nat. Rev. Drug Disc.* **2011,** *10* (9), 698-712.
13. Chow, V. W.; Mattson, M. P.; Wong, P. C.; Gleichmann, M., An Overview of APP Processing Enzymes and Products. *Neuromol. Medicine* **2010,** *12* (1), 1-12.
14. Benilova, I.; Karran, E.; De Strooper, B., The Toxic Aβ Oligomer and Alzheimer's Disease: An Emperor in Need of Clothes. *Nat. Neurosci.* **2012,** *15*, 349-357.
15. Lee, S. J. C.; Nam, E.; Lee, H. J.; Savelieff, M. G.; Lim, M. H., Towards an understanding of amyloid-beta oligomers: characterization, toxicity mechanisms, and inhibitors. *Chem. Soc. Rev.* **2017,** *46* (2), 310-323.
16. Cline, E. N.; Bicca, M. A.; Viola, K. L.; Klein, W. L., The Amyloid-β Oligomer Hypothesis: Beginning of the Third Decade. *J. Alz. Dis.* **2018,** *64*, S567-S610.
17. Nguyen, P. H.; Ramamoorthy, A.; Sahoo, B. R.; Zheng, J.; Faller, P.; Straub, J. E.; Dominguez, L.; Shea, J.-E.; Dokholyan, N. V.; De Simone, A.; Ma, B.; Nussinov, R.; Najafi, S.; Ngo, S. T.; Loquet, A.; Chiricotto, M.; Ganguly, P.; McCarty, J.; Li, M. S.; Hall, C.; Wang, Y.; Miller, Y.; Melchionna, S.; Habenstein, B.; Timr, S.; Chen, J.; Hnath, B.; Strodel, B.; Kayed, R.; Lesné, S.; Wei, G.; Sterpone, F.; Doig, A. J.; Derreumaux, P., Amyloid Oligomers: A Joint Experimental/Computational Perspective on Alzheimer's Disease, Parkinson's Disease, Type II Diabetes, and Amyotrophic Lateral Sclerosis. *Chem. Rev.* **2021,** *121* (4), 2545-2647.
18. Ciudad, S.; Puig, E.; Botzanowski, T.; Meigooni, M.; Arango, A. S.; Do, J.; Mayzel, M.; Bayoumi, M.; Chaignepain, S.; Maglia, G.; Cianferani, S.; Orekhov, V.; Tajkhorshid, E.; Bardiaux, B.; Carulla, N., Abeta(1-42) tetramer and octamer structures reveal edge conductivity pores as a mechanism for membrane damage. *Nat. Commun.* **2020,** *11* (1), 3014.

19. Aliyan, A.; Cook, N. P.; Martí, A. A., Interrogating Amyloid Aggregates using Fluorescent Probes. *Chem. Rev.* **2019,** *119* (23), 11819-11856.
20. Teoh, C. L.; Su, D.; Sahu, S.; Yun, S. W.; Drummond, E.; Prelli, F.; Lim, S.; Cho, S.; Ham, S.; Wisniewski, T.; Chang, Y. T., Chemical Fluorescent Probe for Detection of Abeta Oligomers. *J. Am. Chem. Soc.* **2015,** *137* (42), 13503-9.
21. Li, Y.; Xu, D.; Sun, A.; Ho, S. L.; Poon, C. Y.; Chan, H. N.; Ng, O. T. W.; Yung, K. K. L.; Yan, H.; Li, H. W.; Wong, M. S., Fluoro-substituted cyanine for reliable in vivo labelling of amyloid-beta oligomers and neuroprotection against amyloid-beta induced toxicity. *Chem. Sci.* **2017,** *8* (12), 8279-8284.
22. Lv, G.; Sun, A.; Wei, P.; Zhang, N.; Lan, H.; Yi, T., A spiropyran-based fluorescent probe for the specific detection of beta-amyloid peptide oligomers in Alzheimer's disease. *Chem. Comm.* **2016,** *52* (57), 8865-8868.
23. Li, Y.; Yang, J.; Liu, H.; Yang, J.; Du, L.; Feng, H.; Tian, Y.; Cao, J.; Ran, C., Tuning the stereo-hindrance of a curcumin scaffold for the selective imaging of the soluble forms of amyloid beta species. *Chem. Sci.* **2017,** *8* (11), 7710-7717.
24. Lv, G. L.; Sun, A. Y.; Wang, M. Q.; Wei, P.; Li, R. H.; Yi, T., A novel near-infrared fluorescent probe for detection of early-stage Ab protofibrils in Alzheimer's disease. *Chem. Commun.* **2020,** *56* (11), 1625-1628.
25. Yang, J.; Zeng, F.; Li, X.; Ran, C.; Xu, Y.; Li, Y., Highly Specific Detection of Aβ Oligomers in Early Alzheimer's Disease by a Near-Infrared Fluorescent Probe with a “V-shaped” Spatial Conformation. *Chem. Commun.* **2020,** *56* (4), 583-586.
26. Liu, Y.; Wolstenholme, C. H.; Carter, G. C.; Liu, H.; Hu, H.; Grainger, L. S.; Miao, K.; Fares, M.; Hoelzel, C. A.; Yennawar, H. P.; Ning, G.; Du, M.; Bai, L.; Li, X.; Zhang, X., Modulation of Fluorescent Protein Chromophores To Detect Protein Aggregation with Turn-On Fluorescence. *J. Am. Chem. Soc.* **2018,** *140* (24), 7381-7384.
27. Wolstenholme, C. H.; Hu, H.; Ye, S.; Funk, B. E.; Jain, D.; Hsiung, C.-H.; Ning, G.; Liu, Y.; Li, X.; Zhang, X., AggFluor: Fluorogenic Toolbox Enables Direct Visualization of the Multi-Step Protein Aggregation Process in Live Cells. *J. Am. Chem. Soc.* **2020,** *142* (41), 17515-17523.

28. Alies, B.; Eury, H.; Essassi, E. M.; Pratviel, G.; Hureau, C.; Faller, P., Concept for Simultaneous and Specific in Situ Monitoring of Amyloid Oligomers and Fibrils via Förster Resonance Energy Transfer. *Anal. Chem.* **2014,** *86* (23), 11877-11882.
29. Jiang, B.; Aliyan, A.; Cook, N. P.; Augustine, A.; Bhak, G.; Maldonado, R.; Smith McWilliams, A. D.; Flores, E. M.; Mendez, N.; Shahnawaz, M.; Godoy, F. J.; Montenegro, J.; Moreno-Gonzalez, I.; Martí, A. A., Monitoring the Formation of Amyloid Oligomers Using Photoluminescence Anisotropy. *J. Am. Chem. Soc.* **2019,** *141* (39), 15605-15610.
30. Sun, L.; Cho, H.-J.; Sen, S.; Arango, A. S.; Bandara, N.; Huang, Y.; Huynh, T. T.; Rogers, B. E.; Tajkhorshid, E.; Mirica, L. M., Amphiphilic Distyrylbenzene Derivatives as Potential Therapeutic and Imaging Agents for the Soluble Amyloid-β Oligomers in Alzheimer's Disease. *J. Am. Chem. Soc.* **2021,** *143*, 10462-10476.
31. Yu, Z.; Guo, W.; Patel, S.; Cho, H.-J.; Sun, L.; Mirica, L. M., Amphiphilic stilbene derivatives attenuate the neurotoxicity of soluble Aβ42 oligomers by controlling their interactions with cell membranes. *Chem. Sci.* **2022**, DOI: 10.1039/D2SC02654F.
32. Rai, H.; Gupta, S.; Kumar, S.; Yang, J.; Singh, S. K.; Ran, C.; Modi, G., Near-Infrared Fluorescent Probes as Imaging and Theranostic Modalities for Amyloid-Beta and Tau Aggregates in Alzheimer's Disease. *J. Med. Chem.* **2022,** *65* (13), 8550-8595.
33. Liu, H. W.; Yang, J.; Wang, L. T.; Xu, Y. G.; Zhang, S. Y.; Lv, J.; Ran, C. Z.; Li, Y. Y., Targeting beta-amyloid plaques and oligomers: development of near-IR fluorescence imaging probes. *Future Med. Chem.* **2017,** *9* (2), 179-198.
34. Suzuki, N.; Wakioka, M.; Ozawa, F.; Yamaguchi, S., A Near-Infrared Emissive π-Conjugated Polymer Consisting of an Excited-State Intramolecular Proton Transfer Unit. *Asian J. Org. Chem.* **2020,** *9* (9), 1326-1332.
35. See Supporting Information.
36. Demchenko, A. P.; Tang, K.-C.; Chou, P.-T., Excited-state proton coupled charge transfer modulated by molecular structure and media polarization. *Chem. Soc. Rev.* **2013,** *42* (3), 1379-1408.

37. Wu, X.; Sun, X.; Guo, Z.; Tang, J.; Shen, Y.; James, T. D.; Tian, H.; Zhu, W., In Vivo and in Situ Tracking Cancer Chemotherapy by Highly Photostable NIR Fluorescent Theranostic Prodrug. *J. Am. Chem. Soc.* **2014,** *136* (9), 3579-3588.
38. Storr, T.; Merkel, M.; Song-Zhao, G. X.; Scott, L. E.; Green, D. E.; Bowen, M. L.; Thompson, K. H.; Patrick, B. O.; Schugar, H. J.; Orvig, C., Synthesis, characterization, and metal coordinating ability of multifunctional carbohydrate-containing compounds for Alzheimer's therapy. *J. Am. Chem. Soc.* **2007,** *129* (23), 7453-7463.
39. Ye, S.; Zhang, H.; Fei, J.; Wolstenholme, C. H.; Zhang, X., A General Strategy to Control Viscosity Sensitivity of Molecular Rotor-Based Fluorophores. *Angew. Chem. Int. Ed.* **2021,** *60* (3), 1339-1346.
40. Fu, W.; Yan, C.; Guo, Z.; Zhang, J.; Zhang, H.; Tian, H.; Zhu, W.-H., Rational Design of Near-Infrared Aggregation-Induced-Emission-Active Probes: In Situ Mapping of Amyloid-β Plaques with Ultrasensitivity and High-Fidelity. *J. Am. Chem. Soc.* **2019,** *141* (7), 3171-3177.
41. Cheng, Y.; Zhu, B.; Deng, Y.; Zhang, Z., In Vivo Detection of Cerebral Amyloid Fibrils with Smart Dicynomethylene-4H-Pyran-Based Fluorescence Probe. *Anal. Chem.* **2015,** *87* (9), 4781-4787.
42. Cheng, Y.; Zhu, B.-y.; Li, X.; Li, G.-b.; Yang, S.-y.; Zhang, Z.-r., A pyrane based fluorescence probe for noninvasive prediction of cerebral β-amyloid fibrils. *Biorg. Med. Chem. Lett.* **2015,** *25* (20), 4472-4476.
43. Klein, W. L.; Krafft, G. A.; Finch, C. E., Targeting small A beta oligomers: the solution to an Alzheimer's disease conundrum? *Trends Neurosci.* **2001,** *24* (4), 219-224.
44. Su, D.; Diao, W.; Li, J.; Pan, L.; Zhang, X.; Wu, X.; Mao, W., Strategic Design of Amyloid-β Species Fluorescent Probes for Alzheimer's Disease. *ACS Chem. Neurosci.* **2022,** *13* (5), 540-551.
45. Förster, T.; Hoffmann, G., Die Viskositätsabhängigkeit der Fluoreszenzquantenausbeuten einiger Farbstoffsysteme. **1971,** *75* (1-2), 63-76.
46. Stsiapura, V. I.; Maskevich, A. A.; Kuzmitsky, V. A.; Uversky, V. N.; Kuznetsova, I. M.; Turoverov, K. K., Thioflavin T as a Molecular Rotor: Fluorescent Properties of Thioflavin T in Solvents with Different Viscosity. *J. Phys. Chem. B* **2008,** *112* (49), 15893-15902.

47. Biancalana, M.; Koide, S., Molecular mechanism of Thioflavin-T binding to amyloid fibrils. *Biochim. Biophys. Acta* **2010,** *1804* (7), 1405-1412.

48. Oakley, H.; Cole, S. L.; Logan, S.; Maus, E.; Shao, P.; Craft, J.; Guillozet-Bongaarts, A.; Ohno, M.; Disterhoft, J.; Van Eldik, L.; Berry, R.; Vassar, R., Intraneuronal beta-amyloid aggregates, neurodegeneration, and neuron loss in transgenic mice with five familial Alzheimer's disease mutations: potential factors in amyloid plaque formation. *J. Neurosci.* **2006,** *26* (40), 10129-40.

49. Wengenack, T. M.; Whelan, S.; Curran, G. L.; Duff, K. E.; Poduslo, J. F., Quantitative histological analysis of amyloid deposition in Alzheimer's double transgenic mouse brain. *Neuroscience* **2000,** *101* (4), 939–944.

50. Wilcock, D. M.; Gordon, M. N.; Morgan, D., Quantification of cerebral amyloid angiopathy and parenchymal amyloid plaques with Congo red histochemical stain. *Nature Protocols* **2006,** *1*, 1591–1595.

51. Wager, T. T.; Chandrasekaran, R. Y.; Hou, X.; Troutman, M. D.; Verhoest, P. R.; Villalobos, A.; Will, Y., Defining Desirable Central Nervous System Drug Space through the Alignment of Molecular Properties, in Vitro ADME, and Safety Attributes. *ACS Chem. Neurosc.* **2010,** *1* (6), 420-434.

52. Wang, Y.; Huynh, T. T.; Bandara, N.; Cho, H.-J.; Rogers, B. E.; Mirica, L. M., 2-(4-Hydroxyphenyl)benzothiazole Dicarboxylate Ester TACN Chelators for 64Cu PET imaging in Alzheimer's Disease. *Dalton Trans.* **2022,** *51*, 1216–1224.

53. Wang, Y.; Huynh, T. T.; Cho, H.-J.; Wang, Y.-C.; Rogers, B. E.; Mirica, L. M., Amyloid β-Binding Bifunctional Chelators with Favorable Lipophilicity for 64Cu Positron Emission Tomography Imaging in Alzheimer's Disease. *Inorg. Chem.* **2021,** *60* (16), 12610-12620.

54. Sharma, A. K.; Schultz, J. W.; Prior, J. T.; Rath, N. P.; Mirica, L. M., Coordination Chemistry of Bifunctional Chemical Agents Designed for Applications in (64)Cu PET Imaging for Alzheimer's Disease. *Inorg. Chem.* **2017,** *56* (22), 13801-13814.

55. Martell, A. E.; Smith, R. M., *Critical Stability Constants*. Plenum: New York, 1976; Vol. IV, p 1.

56. Shen, D.; Jin, W.; Bai, Y.; Huang, Y.; Lyu, H.; Zeng, L.; Wang, M.; Tang, Y.; Wan, W.; Dong, X.; Gao, Z.; Piao, H.-L.; Liu, X.; Liu, Y., Rational Design of Crystallization-Induced-Emission Probes To Detect Amorphous Protein Aggregation in Live Cells. *Angew. Chem. Int. Ed.* **2021,** *60* (29), 16067-16076.

57. Gardner, S. H.; Brady, C. J.; Keeton, C.; Yadav, A. K.; Mallojjala, S. C.; Lucero, M. Y.; Su, S.; Yu, Z.; Hirschi, J. S.; Mirica, L. M.; Chan, J., A General Approach to Convert Hemicyanine Dyes into Highly Optimized Photoacoustic Scaffolds for Analyte Sensing. *Angew. Chem. Int. Ed.* **2021,** *60* (34), 18860-18866.

58. Huang, J.; Jiang, Y.; Li, J.; Huang, J.; Pu, K., Molecular Chemiluminescent Probes with a Very Long Near-Infrared Emission Wavelength for in Vivo Imaging. *Angew. Chem. Int. Ed.* **2021,** *60* (8), 3999-4003.